Solar driven micro-ORC system assessment for residential application

Solar driven micro-ORC system assessment for residential application

Maria Alessandra Ancona, Michele Bianchi, Lisa Branchini, Andrea De Pascale, Francesco Melino, Antonio Peretto, Chiara Poletto*, Noemi Torricelli

Alma Mater Studiorum – University of Bologna
Department of Industrial Engineering, Viale del Risorgimento 2, 40136 Bologna, Italy
E–mail address: chiara.poletto3@unibo.it

ABSTRACT

The purpose of this study is to estimate the electricity production obtainable by coupling an existing kW-size recuperated Organic Rankine Cycle (ORC) prototype with a commercial solar thermal collector to reduce the yearly electricity purchased by a single-family user. A detailed semi-empirical steady-state model, validated against experimental data, is employed for the power plant simulation. The optimal sizes of both the collector surface and the storage tanks were assessed considering that a solar collector surface larger than 32.25 m² would lead the micro-ORC working in off-design conditions; while storage volumes higher than 6000 l become too large to be completely exploited.

Then, different low global warming potential fluids and blends were simulated for comparison with HFC-134a, the reference fluid for low-temperature ORC. Results show that the integrated system working with R134a can cover approximately 39% of the yearly electricity demand, corresponding to more than 1150 kWh. The replacement of R134a with the alternative fluids results in a penalization in the output electric power, related to thermodynamic properties such as density, liquid viscosity, and latent heat. Indeed, with R1234yf barely 16% (466 kWh) of the yearly electricity demand is covered; whilst the blend R513A allows to reach only 17.5% (525 kWh).

KEYWORDS

Micro-ORC; thermal solar; R134a; low-GWP fluids; semi-empirical model; residential application.

1. Introduction

During the last decades, the release of ever greater quantities of carbon dioxide has contributed to significantly increase the greenhouse effect and, consequently, temperatures and climate are being altered. Hence, the research for measures and solutions to reduce the amount of greenhouse gases released into the atmosphere is one of the main challenges of the current century [1].

In this context, the Organic Rankine Cycle (ORC) technology might play a pivotal role in the power generation from low-grade heat sources (i.e. below 300 °C): the technology may be used to produce electrical energy recovering waste heat from industrial processes, which would otherwise be dissipated. In addition, ORC systems may be a solution to exploit renewable low-temperature heat sources such as geothermal, concentrated solar thermal, and biomass combustion [2]. In particular, technology in the field of renewable energy is advancing quickly, in order to boost a deeper penetration of Renewable Energy Sources (RES) to allow the transition towards sustainable energy systems [3]. Moreover, according to Pereira et al. [4], ORC seems to be the most suitable and promising technology to be used in cogeneration plants in residential areas, the so-called Combined Heat and Power production (micro-CHP) system.

Quoilin et al., in their survey [5], have made an overview of the various ORC applications: such technology is consolidated to recover low-temperature waste heat, released by some industrial

Nomenclature		*Subscripts*	
A	Area [m²]	amb	ambient
AU	Global heat exchange coefficient [W K⁻¹]	c	condensation
c_p	Specific heat at constant pressure [J kg⁻¹ K⁻¹]	con	conversion
h	Specific enthalpy [J kg⁻¹]	el	electric
I	Irradiation [W K⁻¹]	ex	exhaust
L	Length [m]	H2O	water
$\dot{m}$	Mass flow rate [kg s⁻¹]	in	inlet
N	Rotation speed [rpm]	out	outlet
Nu	Nusselt number [-]	pump	pump
p	Pressure [bar, Pa]	ref	reference
Q	Quality [-]	sat	saturation
$\dot{Q}$	Thermal power [W]	tot	total
s	Specific entropy [J kg⁻¹ K⁻¹]	v	vaporization
SC	Subcooling [K, °C]	wf	working fluid
SH	Superheating [K, °C]		
T	Temperature [K, °C]	*Abbreviations*	
U	Global heat exchange coefficient [W m⁻¹ K⁻¹]	CD	condenser
V	Volume [m³]	COLL	collector
$\dot{V}$	Volume flow rate [L s⁻¹]	EV	evaporator
$\dot{W}$	Power [W]	EXP	expander
α	Convective heat transfer coefficient [W m⁻¹ K⁻¹]	liq	liquid
Δ	Difference [-]	PP	pump
ε	Heat exchanger efficiency [-]	REC	recuperator
η	Efficiency [-]	vap	vapour
λ	Thermal conductivity [W m⁻¹ K⁻¹]		
μ	Dynamic viscosity [Pa s]		
ρ	Density [kg m⁻³]		

processes, and to exploit geothermal sources, with the advantages of the programmability and the continuity, and biomass, widely available in many agricultural and industrial processes.

ORC systems represent an interesting solution also to exploit solar radiation, by obtaining thermal energy through solar collectors: Dickes et al. [6] analysed and reviewed some of the most interesting and technologically innovative solutions of solar ORC. Solar thermal seems to be the most suitable renewable energy source to be applied in residential areas [4][7], to which micro-generation technologies (such as micro-ORC technology) are aimed. Solar thermal is characterized by: i) medium-low temperatures (<130 °C), ii) high reliability, iii) ease of use and maintenance, iv) compact size and v) the possibility of using different fluids for the heat exchange.

In solar applications, the main disadvantages are the non-programmability of the source and the oscillation of its intensity. In this regard, Soulis et al. [8] found out that the solar radiation variation is not only a function of the latitude but also of the altitude, as it affects the climate variability: this wide spatial variability on the received solar radiation deeply influences the operation efficiency and the produced power of an integrated system that includes solar collectors combined with an ORC engine.

The ORC technology is quite mature for medium and large size applications, while it is still at the prototypal stage as far as micro-generation (plants not exceeding 15-20 kW) is concerned [9]. Since plants of this size are particularly interesting in the residential sector, scientific research is aimed at improving the performance of micro-ORC plants, both analyzing the influence of the working and environmental conditions [10], and developing dynamic control strategies to deal with solar radiation fluctuations.

Few studies have been conducted about solar thermal coupled with ORC technology. Lombardo et al. [11] proposed a dynamic model of a small-sized trigeneration system intended for residential use: it consists of a solar collector, the prototypal micro-ORC test rig considered in the current study, and an absorption refrigeration system. In this study, the Authors highlight the promising features of ORC technology in a trigeneration plant, which has an overall efficiency of 63%.

Calise et al. [12] presented a detailed techno-economic analysis of a prototypal small-scale solar CHP system, based on the coupling of evacuated flat-plate solar thermal collectors with a small ORC. The system results to be economically feasible for the majority of locations in the Mediterranean area. Roumpedakis et al. [13] proposed the exergetic and economic performance assessment of a solar-driven small-scale ORC for application in the South-East Mediterranean region, under multiple scenarios: Authors carried out the analysis considering three collectors typologies working at a different temperature, a wide range of working fluids and different installation sites.

Another interesting domestic scale solar-ORC system is proposed by Kutlu et al. [14], in which the ORC is coupled with a vapour compression cycle (VCC) to work in three different modes: the ORC-VCC system uses solar radiation to produce electric power and cooling in the summertime, power and heating or just heating in the wintertime. Quoilin et al. in their work [15] presented an innovative reversible energy conversion system for domestic application: the system can work either as an ORC unit or a heat pump (HP), depending on the weather conditions (irradiation and ambient temperature) and the heat required in the building.

Liu et al. [16] developed a dynamic fuzzy logic control strategy to maximize the solar radiation absorption, increase the electric power output and improve the thermal efficiency: Authors modelled their non-recuperative 1-kWe ORC test facility using Dymola software in Modelica environment and virtually connected the model with the output thermal power of a solar field simulated in Simulink.

Furthermore, solar systems can easily be integrated into hybrid solutions in which different renewable energy sources may compensate and overcome the drawbacks of the individual system. In this regard, Ciani Bassetti et al. [17] proposed a detailed design and off-design model of a real hybrid geothermal-solar power plant composed of a parabolic trough collector solar field and an air-cooled binary cycle geothermal plant: they showed an increase in the system efficiency and the annual net output power.

Another crucial aspect of the research in the ORC field is the selection of the working fluid, affecting the system design and performance [18]. The selection of the working fluid for the ORC technology is critical since the fluid must not only have thermophysical properties that match the application, but also meet safety requirements and economic costs [19]. Since the great effect on the system operation and energy efficiency, and since the impact on the environment, some procedures have been developed to compare the performances of pure working fluids [20]. Tchanche et al. [21] comparatively assessed the thermodynamic and environmental properties of a few fluids for small scale solar applications.

More in detail, the most common fluids employed for low-temperature applications are refrigerants belonging to HydroFluoroCarbons (HFCs) category [22][23]. Refrigerants seem to be very performing for these applications thanks to their thermodynamic properties [24]: the low critical temperature allows to exploit heat available at relatively low temperature, and the positive or null slope of the vapour saturation limit curve allows to perform a dry expansion, even without superheating the working fluid. One more advantage of refrigerants is related to the high density, which results in more compact system layouts and components.

Critical issues related to HFCs are that they present a high Global Warming Potential (GWP), meaning that, if released into the environment, they contribute to increase the amount of greenhouse gases present in the atmosphere. Possible modern substitutes for HFCs have been identified in the HydroFluoroOlefines (HFOs), which present similar properties to HFCs, but much lower GWP values. A temporary solution to smooth the transition to HFOs working fluids lies in blends, made up of hydrofluorocarbons and hydrofluoroolefines [25][26]. Molés et al. [27] carried out a comparison among the predicted ORC performances of two low-GWP fluids (R1234yf and R1234ze) and R134a.

However, some studies reveal that low-GWP fluids could not always guarantee the same performance as commonly used fluids [28]. Wang and Zhao [29] investigated the possibility of using zeotropic mixtures instead of pure fluids for power generation in low-temperature solar Rankine cycles. Abadi et al. [30] showed that a new zeotropic mixture of R245fa 60% / R134a 40% increases the power output compared to an identical ORC with pure R245fa, despite working at a lower pressure ratio.

1.1. Contribution of this paper

Based on the above literature review, just a few studies have been published about the application of the ORC technology to the solar thermal energy source for residential use. Furthermore, to the Authors' knowledge, in current literature, there are no available works investigating the performance of new generation fluids (HFOs) and their mixtures when used in solar applications at very low temperatures. Thus, the purpose of this study is to enrich the present literature on this topic by comparing the performance that might be reached, with low-GWP working fluids, by coupling an existing micro-ORC prototype system with a commercial solar collector.

The Authors propose an extension of the detailed steady-state simulation model of the aforementioned system, already developed and validated in previous works [22][31]. Overall estimation of the annual energy production when it is applied to a residential building in the Italian town of Bologna is performed. From historical data on solar radiation, it was possible to estimate the average irradiation profile of each month and to evaluate the performance of the system at various times of the year. A comparison was made among the performance of the system obtained by simulating its behaviour when R134a, the fluid currently available in the plant, and five low-GWP alternatives (R1234yf, R1234ze(E), R1243zf, R513A, R515A) are used as working fluids.

The first part of the article is dedicated to a brief description of the approach adopted to model the system, highlighting the key features of each sub-model and the way they are linked together. Compared to the previous Authors' studies, the solar collector and the hot water circuit models and regulation strategy are integrated into the calculation code. The working fluid selection, since one of the most critical design aspects in the ORC technology, is also discussed.

In the second part of the article, the Authors show and comment on the results of the simulations performed by considering the average daily profiles of irradiation and ambient temperature for each month in Bologna: a parametric analysis is carried out by varying the solar collector surface and the storage dimensions to find the couple of parameters which maximize the output electricity production; then a performance comparison is realized with different fluids and mixtures. The discussion is carried out by comparing performance indexes and the annual electricity production obtained with the different fluids.

2. Material and Methods

In this section, a detailed description of the approach adopted to model the system is given. First, the system is described as a whole, and then a focus on each main component modelling is provided. The section ends with an explanation of the fluid selection, and the description of the boundary conditions and the regulation strategy adopted in the simulations.

2.1. Layout and model of the system

The modelled energy system consists of a micro–ORC conceived to supply electric power to a single-family residential user. The system exploits solar radiation through an external circuit made up of a commercial thermal solar collector and a thermal energy storage system (Figure 1).

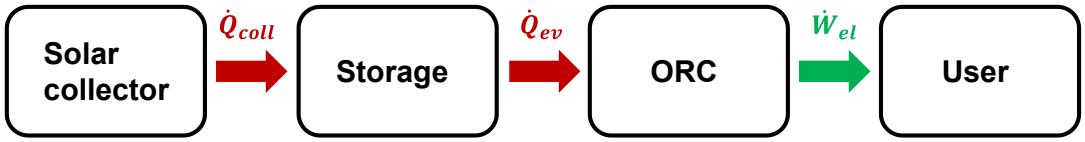

Figure 1. Conceptual scheme of the energy system with main thermal and electric power flows

A thermodynamic steady-state semi-empirical model of the system has been implemented to predict the actual energy performance, under variable input from the solar source. More in detail, the modelled system layout is shown in Figure 2 and described below. According to the scheme, the micro-ORC model introduced in previous works of the Authors [31][22], has been coupled with a heat source circuit model comprising: a flat plate thermal solar collector and two storage tanks, which decouple the solar collector thermal power production from the ORC evaporator thermal demand, depending on the user electricity demand.

The heat transfer fluid is water, which transfers thermal power from the collector to the storage system, and from the storage to the organic working fluid at the ORC evaporator. The solar collector has been sized to work at the nominal point under the reference case study operating conditions, represented by 800 W/m² of irradiance and ambient temperature equal to 20 °C. To ensure the optimal ORC operation, 2 °C of water temperature glide through the evaporator and 2 l/s of water flow rate (for a thermal power of about 16 kW) are considered when sizing the solar collector under the aforementioned boundary conditions.

Under these assumptions, a solar collector capturing surface equal to about 32.25 m^2 is chosen for the case study (more details on the solar collector characteristics are provided in the dedicated paragraph 2.2). The storage tanks size is chosen equal to 6000 l, as a compromise between the desire of realising the ORC operation from the solar radiation fluctuations and the need of limiting the overall dimensions, as a potential residential application (see paragraph 4.2 for further details on the tanks and the solar collector sizing).

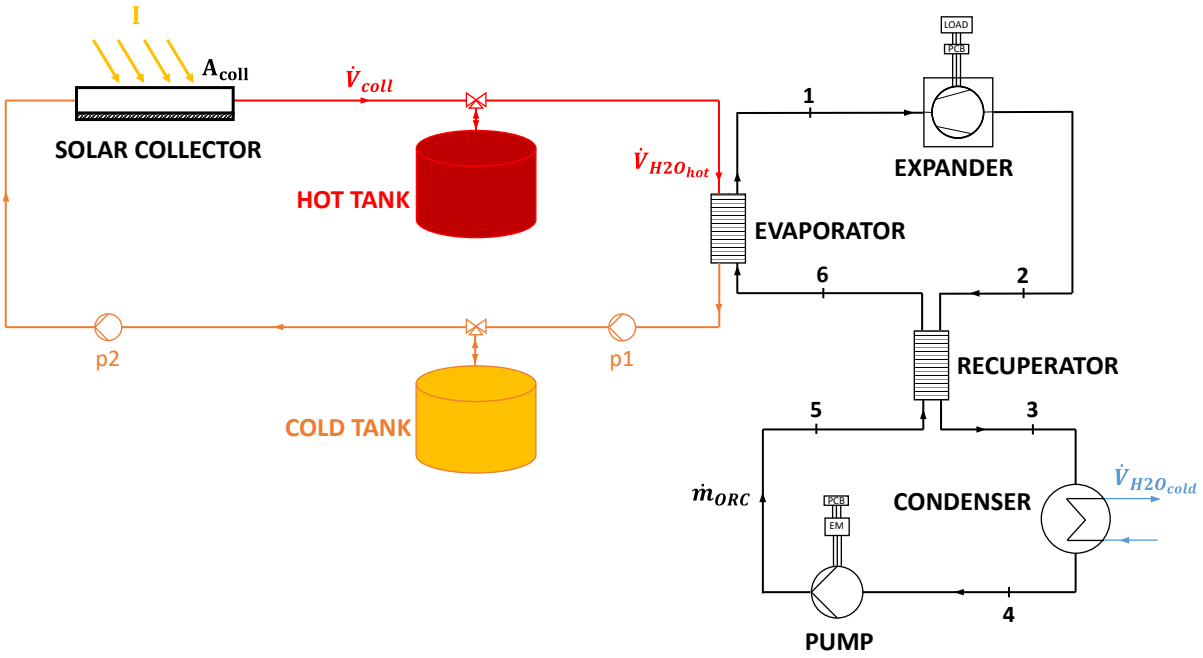

Figure 2. The integrated solar-ORC system layout

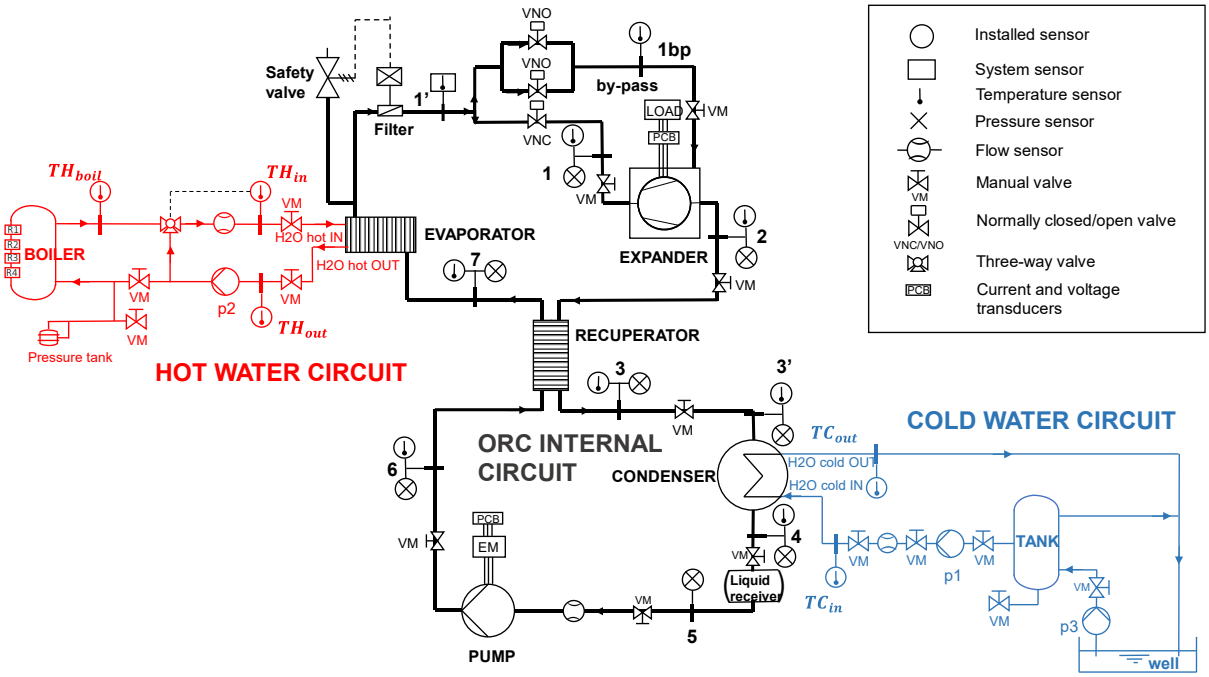

Figure 3. Micro-ORC test bench layout

The micro-ORC performance model is validated by taking as reference the small-scale prototype test rig (Figure 3) developed in the micro-generation laboratory of the University of Bologna [32]. The reference system consists of a kW-size recuperated micro-ORC, conceived for heat source temperature below 100 °C.

The key component of the system is the expander, a prototype of a reciprocating pistons model, directly coupled with the generator, which is connected to an electrical load, made of five pure resistive

loads. The ORC feed pump is an external gear type, driven by an asynchronous electric motor, which is driven by a frequency inverter, allowing a proper regulation of the flow rate of the working fluid.

The heat exchangers are commercial brazed plate (evaporator and recuperator) and shell-and-tube (condenser) heat exchangers. The evaporator has been tested with hot water supplied by an electric heater of 40 kW nominal thermal power (high enough to cover the simulated operation in which the ORC input thermal power is around 16 kW); the condenser has been tested with cold water provided at variable ambient temperature by a well installed in the laboratory [31].

The operating ranges of key variables in which the micro-ORC prototype has been tested and the corresponding performance are reported in Table 1.

Table 1. Micro-ORC tested conditions and power ranges

ORC power output	0 – 1800 W
Hot water temperature	45 – 95 °C
Cold water temperature	14 – 28 °C
ORC mass flow rate	0.05 – 0.14 kg/s
R134a vaporization pressure	11 – 19 bar
R134a condensing pressure	5 – 8 bar

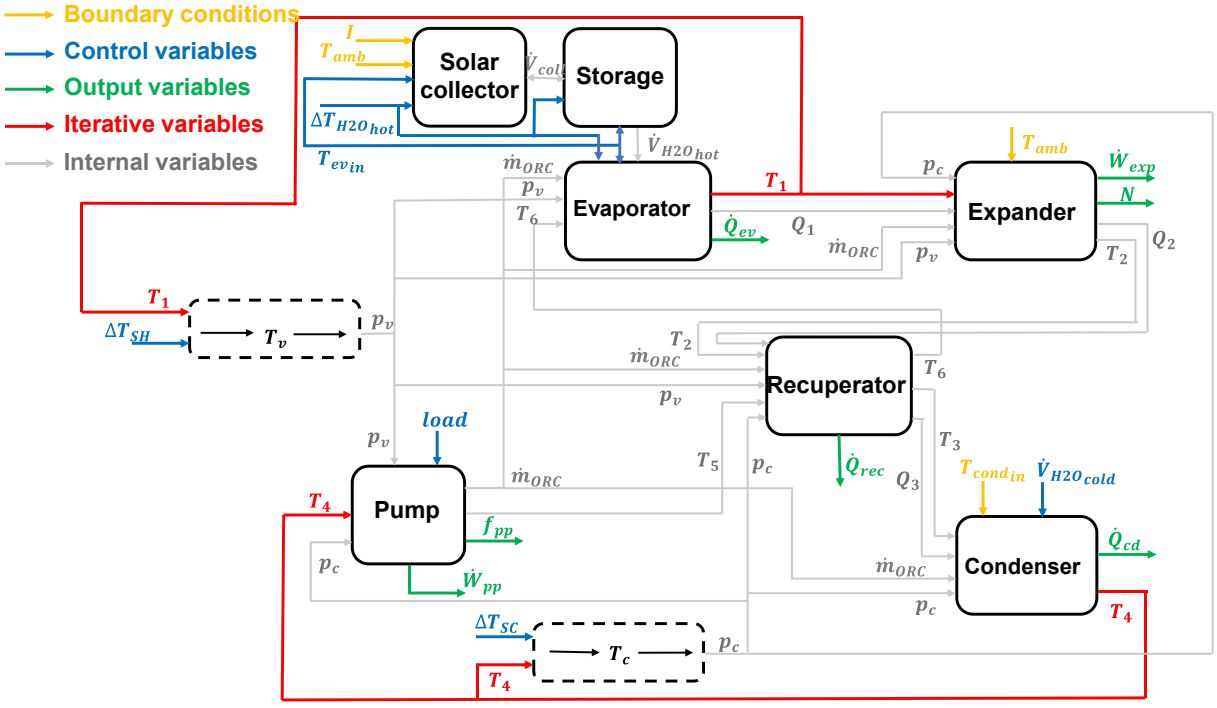

Figure 4. Model block diagram representing the main modelled components of the system and the interconnection variables

Each component of the considered system has been modelled according to a semi-empirical approach with lumped parameters: rather than a constant-efficiency or a polynomial-based model, a

lumped parameters one is more accurate in simulating the performance of ORC systems, with robust prediction in both fitting and extrapolation [33].

The model has been implemented in MATLAB environment; the thermodynamic properties of the fluids have been calculated using REFPROP library [34].

Figure 4 shows a scheme of the system model, highlighting the components sub-models blocks and the involved thermodynamic variables. The components sub-models refer to: the expander; the ORC pump; the evaporator; the recuperator; the condenser; and the thermal solar collector. Each component is modelled as a MATLAB function and validated with experimental data collected during the reference rig experimental tests, using R134a as ORC working fluid [32]. The sub-models functions are linked together through the respective input and output variables, representing the thermodynamic conditions of the fluid at the inlet and outlet of the different components.

The inputs of the model are the boundary conditions of the system and the variables that can be controlled from the outside: the boundary conditions are the solar radiation (I), the ambient temperature (T_{amb}), and the cold source temperature ($T_{H2O\,cold}$); whilst the control variables are the evaporator inlet temperature ($T_{ev_{in}}$), the hot water temperature difference between the inlet and the outlet of the evaporator ($\Delta T_{H2O\,hot}$), the superheating level at the expander inlet (ΔT_{SH}), the electric load ($load$), the water volumetric flow rate at the condenser inlet ($\dot{V}_{H2O\,cold}$), and the subcooling level at the condenser outlet (ΔT_{SC}).

Since the model is formulated as two levels implicit problem, its solution is determined through an iterative process with two iterative variables: the expander inlet temperature (T_1) and the condenser outlet temperature (T_4).

The output variables are the expander output power ($\dot{W}_{exp}$) and its shaft rotational speed (N), the pump absorbed power ($\dot{W}_{pp}$) and its frequency (f_{pp}), the thermal input provided at the evaporator ($\dot{Q}_{ev}$), the condenser discharged heat ($\dot{Q}_{cd}$), and the thermal power exchanged in the recuperator ($\dot{Q}_{rec}$).

2.2. Solar collector model

According to Garcia-Saez et al. [35], a 0-dimensional approach was adopted to model the flat solar collector behaviour in quasi-static equilibrium conditions. The thermal solar collector model reproduces the energy balance between the incident solar radiation (I) hitting the absorbing surface (A_{coll}), and the thermal power transferred to the water crossing the component (Figure 5).

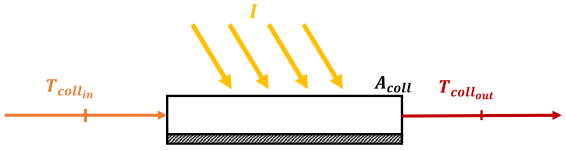

Figure 5. Scheme of the flat-plate thermal solar collector

Heat absorbed at the collector surface, $\dot{Q}_{coll}$, is evaluated through Eq. (1):

$$\dot{Q}_{coll} = \eta_{coll} \cdot I \cdot A_{coll} \tag{1}$$

The collector efficiency, η_{coll}, is given by the following equation:

$$\eta_{coll} = \eta_0 - a_1 \cdot \frac{T_{coll_{in}} - T_{amb}}{I} - a_2 \cdot \left(\frac{T_{coll_{in}} - T_{amb}}{I}\right)^2 \tag{2}$$

in which η_0, a_1 and a_2 are parameters provided by the collector catalogue [36]; $T_{coll_{in}}$ is the water temperature at the solar collector inlet, which is equal to the water temperature at the evaporator outlet ($T_{ev_{out}}$); and T_{amb} is the ambient temperature.

Table 2 reports the solar collector's main specifications for a single panel, including the cited parameters. It can be noticed that the solar collector capturing surface size (equal to about 32.25 m²) is obtained by assembly of 15 panels of the chosen model. The solar collector characteristic curve, obtained from Eq. (2), is also shown in Figure 6.

Table 2. Thermal solar collector single panel specifications

Surface [m²]		Absorber			Stagnation Temperature	Dimensions [mm]			Weight
Total	Absorbent	η_0	a_1 [W/ (m²K)]	a_2 [W/ (m²K²)]	[°C]	L	H	P	[kg]
2.57	2.15	0.839	3.47	0.0106	214	2077	1238	100	46

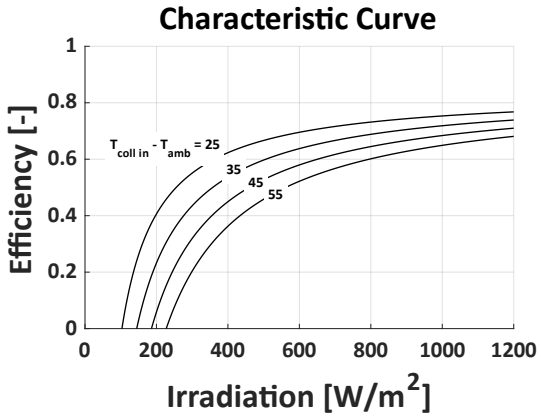

Figure 6. Thermal solar collector characteristic curves

The energy balance on the collector provides, as output, the water temperature value at the inlet of the evaporator, $T_{ev_{in}}$, which is equal to the water temperature at the outlet of the solar collector $T_{coll_{out}}$ (Eq. (3)):

$$T_{coll_{out}} = T_{coll_{in}} + \frac{\dot{Q}_{coll}}{\dot{V}_{H2O_{hot}} \cdot \rho_{H2O_{hot}} \cdot c_{p_{H2O_{hot}}}} \quad (3)$$

The effects of radiative losses, condensation, axial conduction and heat dissipation to the external environment have been neglected.

2.3. Storage model

The storage tanks are modelled as containers which are filled or emptied, according to the mass balance between the inlet and the outlet flow rate, depending on the solar collector and the evaporator operation.

In particular, when the water flow rate crossing the solar collector, $\dot{V}_{coll}$, is higher than the evaporator demanded flow rate, $\dot{V}_{H2O_{hot}}$, the hot tank is filled, and the cold tank is emptied of the same water volume; conversely, when the solar collector water flow rate decreases under the evaporator request, the hot tank turns to be emptied and the cold tank is filled. According to the balances presented

in Eq. (4) and Eq. (5), the water volume values inside the hot ($V_{hot_{tank_0}}$) and cold tank ($V_{cold_{tank_0}}$) are updated to their new values ($V_{hot_{tank}}$ and $V_{cold_{tank}}$) after the time $t_{filling/empting}$:

$$V_{hot_{tank}} = V_{hot_{tank_0}} + (\dot{V}_{coll} - \dot{V}_{H2O_{hot}}) \cdot t_{filling/empting} \quad (4)$$

$$V_{cold_{tank}} = V_{cold_{tank_0}} + (\dot{V}_{H2O_{hot}} - \dot{V}_{coll}) \cdot t_{filling/empting} \quad (5)$$

A constraint is imposed to stop the filling (or emptying) when the tank is completely full (or empty). Thermal dissipation through the storage is considered negligible.

2.4. ORC reciprocating piston expander model

The volumetric piston expander is simulated through a grey-box model, validated for the reference reciprocating expander in a previous work of the Authors [37]. As an improvement of the model, in this study the possibility of simulating also a two-phase expansion was added. The model follows a lumped parameters approach as illustrated by the scheme shown in Figure 7.

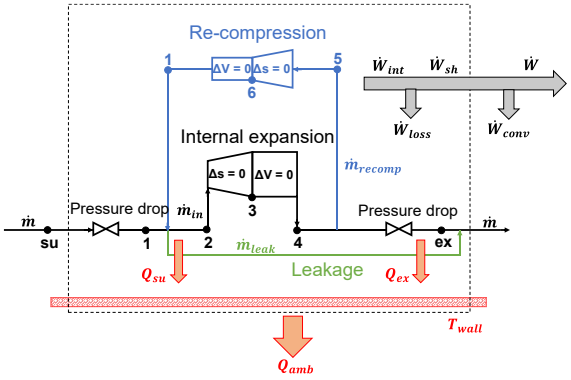

Figure 7. Scheme of the expander model

The function models the cycle performed by the working fluid inside the expander to get the outlet thermodynamic conditions and the output electric power. It is based on equations describing the fluid admission, the internal expansion, the fluid exhaust, the re-compression phenomenon, and additional characteristic power losses.

The fluid admission and exhaust are modelled as the result of two stages each: the first stage is schematized as an isentropic flow through a converging nozzle (Eq. (6)), therefore only the pressure drop is considered; while in the second stage the pressure is assumed to remain constant and only the dissipation of thermal power is taken into account, according to the ε -NTU method (Eq. (7)):

$$\dot{m}_{ORC} = \rho_{su/ex} \cdot A_{su/ex} \cdot \sqrt{2 \cdot |h_{su/ex} - h_{wf}|} \quad (6)$$

$$\dot{Q}_{su/ex} = \varepsilon_{su/ex} \cdot \dot{m}_{in} \cdot c_p \cdot (T_{wf} - T_{wall}) \quad (7)$$

An equation similar to Eq. (6) is also used to estimate the leakage mass flow rate between the cylinder liner wall and the piston.

The internal expansion is schematized as the result of an isentropic expansion followed by a constant volume transformation, for which the isentropic expansion pressure ratio is determined by the built-in volume ratio parameter (see $r_{v_{exp}}$ in Table 3). In case the isentropic expansion ratio is different from the cycle expansion ratio, two different contributions of losses can affect the expander

performance, whether the pressure at the end of the isentropic transformation is higher or lower than the condensing one: namely the under-expansion or the over-expansion process.

The re-compression phenomenon (due to the presence of fluid trapped in the cylinder at the exhaust valve closure) is also modelled as an isentropic compression followed by a constant volume one, involving the mass flow rate, $\dot{m}_{rec}$.

Additional kinds of losses considered by the model are then the heat dissipation through the expander wall, the frictions, and the electro-mechanical conversion losses. Accounting for all these loss contributions, the output electric power is provided by Eq. (8):

$$\dot{W}_{exp} = \left[\dot{m}_{in} \cdot \left(l_{exp_s} + l_{exp_V}\right) - \dot{m}_{rec} \cdot \left(l_{comp_s} + l_{comp_V}\right) - \dot{W}_{loss}\right] \cdot \eta_{con} \quad (8)$$

For a detailed description of the expander model please refer to the previous works of the Authors [31][37]. The input and output variables and the calibrated coefficient of the expander model are reported in Table 3.

Table 3. Expander model parameters

Input		Calibrated Parameters		Output
$\dot{m}_{ORC}$	$AU_{su_{ref}}$	Supply heat transfer coefficient [W/K]	5.65e+05	$\dot{W}_{exp}$
T_1 or Q_1	$AU_{ex_{ref}}$	Exhaust heat transfer coefficient [W/K]	9.23e+05	T_2
p_1	AU_{amb}	Ambient heat transfer coefficient [W/K]	0.96	N
p_2	$r_{v_{exp}}$	Built-in volume ratio [-]	1.459	
T_{amb}	$r_{v_{comp}}$	Re-compression volume ratio [-]	1.25	
	V_0	Clearance volume [m³]	2.32e-08	
	A_{leak}	Equivalent leakage area [m²]	5.51e-06	
	A_{su}	Supply nozzle equivalent section [m²]	1.75e-05	
	$\dot{W}_{loss_{ref}}$	Constant friction losses [W]	0.198	
	$\dot{W}_{loss_N}$	Proportional friction losses [W/min]	1.07e-05	

2.5. ORC pump and circuit resistance model

According to the approach already proposed by the Authors [22][31], the pump function provides the operating point of the machine by crossing the resistance curve of the circuit (Eq. (10)) with the characteristic curve of the pump (Eq. (9)).

The resistance curve depends on the load, $load$, as the increase in the expander resisting load results in an increase in the resisting load on the whole circuit, and on the fluid density, ρ. The characteristic curve of the pump changes instead with its rotational speed, N_{pp} and the fluid dynamic viscosity, μ. Both the pump and the resistance characteristics can be expressed through the relationship between the pump pressure rise, Δp, and the elaborated volume flow rate, $\dot{V}$:

$$\Delta p = (c_1 \cdot N_{pp} + c_2 \cdot \dot{V}) \cdot \mu \quad (9)$$

$$\Delta p = (c_3 \cdot load + c_4) \cdot \dot{V} \cdot \rho \quad (10)$$

Extrapolated curves of the gear pump under exam are shown in Figure 8 in terms of pressure rise versus volumetric flow rate. Calibrated coefficients are listed in Table 4.

Table 4. Pump model parameters

V_{cc} $[m^3]$	$6.2327e-05$
$c_1 = \frac{c_2 \cdot V_{cc}}{60}$ $[-]$	529.4055
c_2 $[m^{-3}]$	$5.0964e+08$
c_3 $\left[\frac{Pa \cdot s}{kg}\right]$	1.5177
c_4 $\left[\frac{Pa \cdot s}{kg}\right]$	53.304

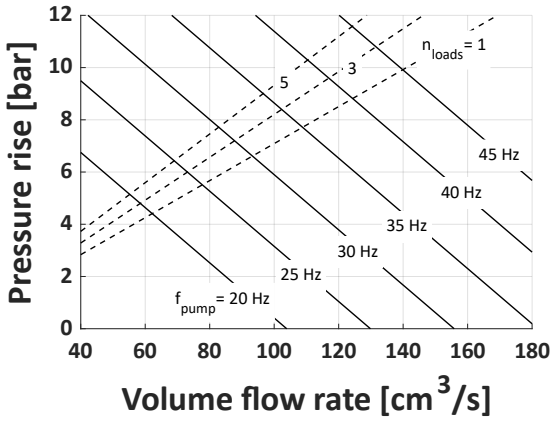

Figure 8. Pump characteristic and circuit resistance

2.6. ORC heat exchangers model

The three heat exchangers (evaporator, recuperator and condenser) are modelled employing a lumped parameters moving boundary approach [38]. Each heat exchanger is decomposed into a number of zones equal to the number of states experienced by the fluid inside the component [39]: in each zone, and for its entire length, the fluid does not change phase. According to this approach, each zone is characterized by a global heat exchange coefficient U_i and a heat transfer surface area A_i through which a certain heat transfer process occurs [40].

The "moving-boundary" approach is particularly accurate as it allows to consider the great variations of the global heat exchange coefficient occurring at the fluid changing phase. The boundaries between consecutive zones are not fixed, but they move depending on the physical state of the fluid. The only constraint is that their sum must be equal to the geometric surface of the component that is a model parameter.

The evaporator and the condenser are modelled as decomposed into three zones (subcooled, two-phase and superheated) each, while in the recuperator a single heat exchange zone is considered. The heat transfer process occurring in the *i-th* zone is obtained using the ε-NTU (*Number of Transfer Units*) method, according to the following three equations:

$$\dot{Q}_i = \varepsilon_i \cdot \dot{m}_{hot} \cdot c_{p_{hot_i}} \cdot \left(T_{in_{hot_i}} - T_{in_{cold_i}}\right) \quad (11)$$

$$\varepsilon_i = \frac{1 - e^{-NTU_i \cdot (1 - C_i^*)}}{1 - C_i^* \cdot e^{-NTU_i \cdot (1 - C_i^*)}} \quad (12)$$

$$NTU_i = \frac{U_i A_i}{C_{min_i}} \quad (13)$$

in which C_i^* is the ratio between the minimum and the maximum thermal capacity.

In the subcooling and the superheating zones, the considered global heat transfer coefficient accounts for the convective coefficient of the working fluid side (α_{wf_i}) and the convective coefficient of the water side (α_{H2O}), Eq. (14):

$$U_i = \left(\frac{1}{\alpha_{wf_i}} + \frac{1}{\alpha_{H2O}}\right)^{-1} \tag{14}$$

The water convective coefficients and the working fluid convective coefficients in the subcooling and superheating zones are evaluated through Dittus-Boelter correlation for forced convection. Instead, in the two-phase zone and the unique zone of the recuperator, the global heat transfer coefficient derives from empirical correlations. In particular, correlations used for the evaporator and the condenser have the form of Eq. (15), while the one used for the recuperator has the form of Eq. (16):

$$U_{ev/cd} = U_{ev/cd\_ref} \cdot \dot{m}^a \cdot \Delta T_{sat}{}^b \cdot \dot{m}_{H2O}{}^c \cdot p_{sat}{}^d \cdot \Delta h_{sat}{}^e \tag{15}$$

$$U_{rec} = U_{rec\_ref} \cdot \dot{m}^a \cdot \Delta T^b \tag{16}$$

In both the above equations the referencing heat transfer coefficients, $U_{ev/cd/rec\_ref}$, and all the exponents have been numerically calibrated to fit the available experimental data. Eq. (15) takes into account the working fluid and water mass flow rates ($\dot{m}$ and $\dot{m}_{H2O}$), the vaporization/condensation pressure (p_{sat}), the temperature difference between the water temperature and the saturation temperature of the working fluid (ΔT_{sat}), and the specific latent heat (Δh_{sat}). Eq. (16) considers just the working fluid mass flow rate ($\dot{m}$) and the inlet temperature difference of the two fluid streams (ΔT). Results of the numerical calibration are reported in Table 5.

Table 5. Heat exchangers models calibrated coefficients

Coefficients	**Evaporator**	**Condenser**	**Recuperator**
U_{ev_ref} $[W/(m \cdot K)]$	0.4046	0.0015	3.7914
a $[-]$	0.9153	0.8894	0.4636
b $[-]$	-0.9607	-0.8284	-0.0186
c $[-]$	-0.0214	-0.0014	
d $[-]$	0.1881	-0.0024	
e $[-]$	1.2056	1.9046	

2.7. Correction of fluid dependent parameters

Even though the majority of the empirical parameters requiring calibration are associated with the components' geometry, some depend on the working fluid thermodynamic characteristics. Indeed, global heat transfer coefficients are working-fluid dependent parameters that have to be corrected to account for the use of fluids different from R134a. For this reason, the global heat transfer coefficients are re-determined by adopting the procedure proposed by Giuffrida [41], when considering different fluids. Since the global heat transfer coefficient is defined as:

$$AU = \frac{Nu \cdot \lambda}{L} \tag{17}$$

where Nu is the Nusselt number, λ is the conductivity and L is the characteristic length. The global heat transfer coefficient for the new fluid, AU_{fluid}, can be determined as function of the reference global heat transfer coefficient, AU_{R134a}, and the fluids properties, by Eq. (18):

$$\frac{AU_{fluid}}{AU_{R134a}} = \frac{Nu_{fluid} \cdot \lambda_{fluid}}{Nu_{R134a} \cdot \lambda_{R134a}} \tag{18}$$

2.8. Fluid selection

In order to investigate in this micro-ORC application low-GWP working fluids [25][26] as alternatives to the basic R134a (GWP=1300 [42]), a comparison of different fluids has been performed. The alternative working fluids selected in this study in line with the current state-of-the-art of low-GWP refrigerants are three different hydrofluoroolefines, namely R1234yf (GWP<1), R1234ze(E) (GWP<1) and R1243zf (GWP<1 [43]), R513A (GWP=573), which is a mixture of 56% R1234yf and 44% R134a, and R515A (GWP=400), which is a mixture of 88% R1234ze(E) and 12% R227.

Very similar thermodynamic properties characterize the aforementioned fluids, namely saturation limit curves in the T-s diagram (Figure 9), critical temperature and pressure, density, viscosity, and latent heat. However, there are small differences that affect the performance of the system: in particular, density and viscosity affect losses due to leakages, and the heat transfer coefficient affects the dissipation of thermal power towards the environment. Table 6 shows density (ρ), viscosity (μ) and latent heat (Δh_{lat}) of each of the considered fluids at typical condensing and evaporating temperature values, respectively related to the ambient temperature and the source temperature.

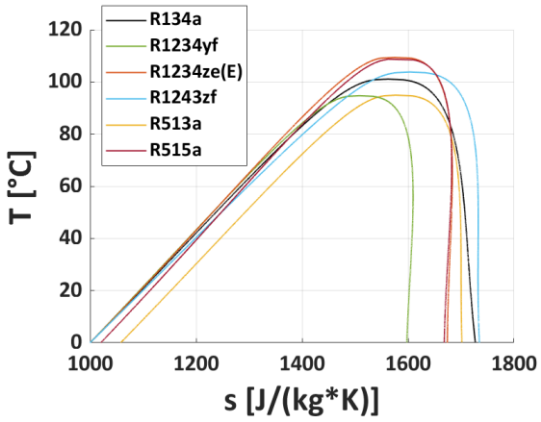

Figure 9. Temperature-entropy diagram comparison of the considered micro-ORC fluids

Table 6. Working fluids thermodynamic properties on saturated curves at typical condensing and evaporating temperatures

	ρ (T=18 °C) [kg/m³]		ρ (T=65 °C) [kg/m³]		μ (T=18 °C) [Pa·s·10⁴]		μ (T=65 °C) [Pa·s·10⁴]		Δh_{lat} (T=18 °C) [kJ/kg]	Δh_{lat} (T=65 °C) [kJ/kg]
	sat. liq.	sat. vap.	sat. liq.	sat. vap.	sat. liq.	sat. vap.	sat. liq.	sat. vap.		
R134a	1233	26.1	1026	100	2.13	0.114	1.15	0.140	184	132
R1234yf	1117	30.9	914	115	1.66	0.111	0.899	0.141	151	104
R1234ze(E)	1186	21.2	1010	80.1	2.08	0.118	1.15	0.148	172	130
R1243zf	999	21.9	837	78.8	1.71	0.111	0.981	0.136	187	138
R513A	1160	30.6	949	116	1.81	0.113	0.966	0.142	162	112
R515A	1210	21.9	1030	82.9	2.12	0.118	1.17	0.147	165	124

2.9. Boundary conditions

In order to estimate the yearly electric energy produced by the considered system, simulations were performed using the monthly averages of the daily hourly profiles of solar radiation. The adopted profiles are based on historical data for the city of Bologna (latitude around 44.5°N), and are provided by UNI 10349 standards [44] for July and September: these profiles are related to solar panels inclined by 30° (in Italy the electricity production is maximized with a tilt angle value between 30° and 35°, depending on the installation location), and south oriented in Bologna.

Normally, solar thermal panels are mounted with an inclination equal to the latitude increased by 15° or 20° to maximize the production of hot water during the winter months [45]. However, since in this case the hot water is used to produce electricity, it is preferable to have an inclination that maximizes its production throughout the year: therefore, it is preferable to adopt the inclination that is normally adopted for photovoltaic panels.

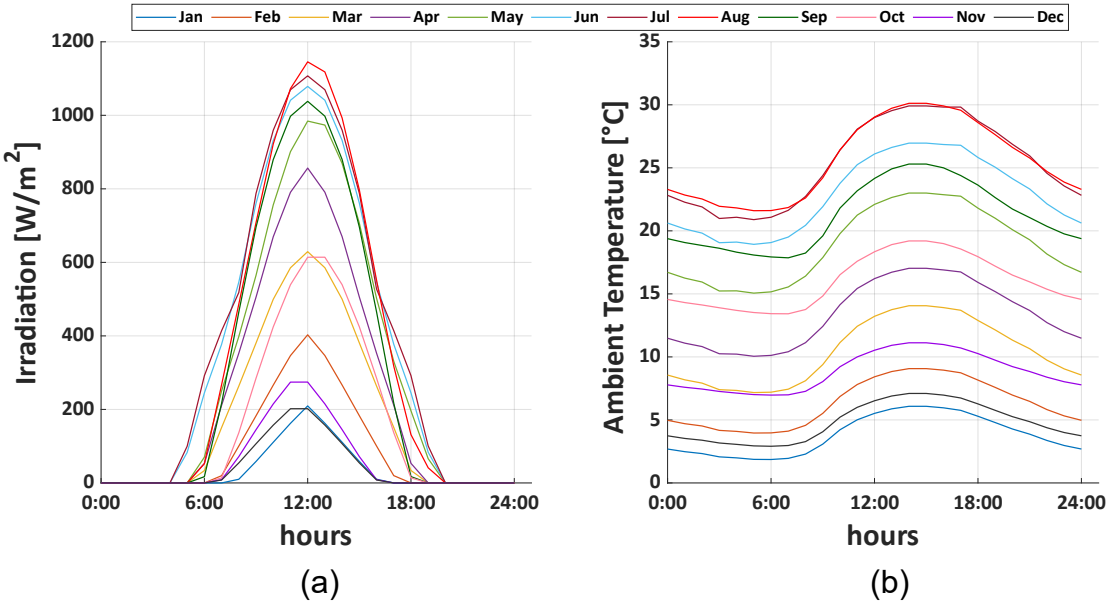

Figure 10. Monthly-averaged Irradiation (a) and Ambient temperature (b) daily profiles

The monthly-averaged daily hourly profile was estimated for all the months of the year (Figure 10a) using the available profiles of July and September, and the monthly average values of daily solar radiation, by ENEA [46]. The corresponding monthly average profiles of the daily hourly ambient temperature are shown in Figure 10b. Then, the ORC performance was simulated with the model on each representative day of the month, assuming the input variables listed in Table 7.

Table 7. Input boundary conditions and control variables

Variable	**Value**					
$load$	3000 W					
$T_{cond_{in}}$	18 °C					
$\dot{V}_{H2O_{cold}}$	2.77 L/s					
ΔT_{SC}	0.5 °C					
$T_{ev_{in}}$	53 - 65 °C					
$\Delta T_{H2O_{hot}}$	2 °C					
ΔT_{SH}	R134a	R1234yf	R1234ze(E)	R1243zf	R513A	R515A
	3°C	15°C	10°C	10°C	20°C	10°C

The ORC regulation strategy is conceived to maximize the ORC system's global efficiency during each operating hour with variable input thermal power from the renewable source. It must be highlighted that the superheating degree at the inlet of the expander is kept constant during the monthly simulations, but it varies according to the chosen fluid, to maximize the electric power output. The evaporator water temperature glide is kept constant and always equal to 2°C, whilst the evaporator water inlet temperature is kept fixed throughout the month, but it takes a different value each month depending on the average monthly irradiance.

The system performance and the electricity production are calculated on an hourly basis, according to a compromise between the need to appreciate the daily and yearly variability, and the need to keep low computational costs. Indeed, hourly data allow to detect the daily solar radiation (and the electric power output) trend without exponentially increasing the computational time and cost. Furthermore, the available irradiation and ambient temperature data are monthly averages, so a narrower discretization would not increase the accuracy of the simulated electricity production. Observing Figure 10, the hourly discretization allows to appreciate daily variations, and the monthly averages are sufficient to appreciate yearly variations.

2.10. Hot water flow rates regulation strategy

The water flow rate through the solar collector is regulated according to the solar radiation, whilst the evaporator water flow rate is attempted to be kept as close as possible to the reference conditions (2 l/s), within the limits of the storage tanks capacity. Both the water flow rates through the solar collector and the evaporator are regulated by a control system which takes into account the value of the current solar radiation and the degree of filling of the storage tanks.

More in detail, first of all, the hot water control system checks if the irradiance value is null or not:

- In case the solar radiation is absent, the control system checks if the hot storage tank is empty or not: if it is empty, no water flow rates are set up; otherwise, a water flow rate of 1.0 l/s (reference value) is set up in the loop crossing the evaporator, until the hot tank is not emptied.
- In case the solar radiation is present, the control system regulates the hot water flow rate crossing the solar collector in such a way as to keep a glide of 2°C. The water flow rate through the evaporator follows the water flow rate through the collector for values higher than 0.4 l/s and

lower than 2.0 l/s. If the water flow rate through the collector is lower than 0.4 l/s, the ORC is kept off or works with a water flow rate higher than 0.4 l/s, depending on the grade of filling of the storage. If the water flow rate through the collector is higher than 2.0 l/s, the ORC works with a water flow rate of 2.0 l/s and the hot tank is filled.

To summarize, the control system tries to keep the ORC operation as close as possible to the reference operating condition to maximize the ORC efficiency. In case the solar irradiance overcomes the reference value of 800 W/m², the thermal power transferred to water across the solar collector is higher than the reference value (16 kW) exchanged in the evaporator: this means that the solar collector flow rate is higher than the evaporator flow rate, so the energy surplus is collected into the hot storage tank. On the contrary, when the solar radiation is lower than 800 W/m² or null, the evaporator demands a water flow rate greater than the one crossing the collector: so, the hot tank is emptied to satisfy the request, and the water surplus at the outlet of the evaporator is stored in the cold tank.

Figure 11 shows the filling and emptying of the storage tanks resulting in a variable state of charge throughout the day. In the first hours of the day, with rising thermal power from the sun but low irradiation intensity, the ORC system is kept off and the heated water is entirely collected inside the hot tank (while the cold tank is being emptied). The ORC is switched on when the minimum ORC output power conditions are reached; the hot tank continues to be filled during the central hours of the day, and eventually, it is emptied during the afternoon and the evening.

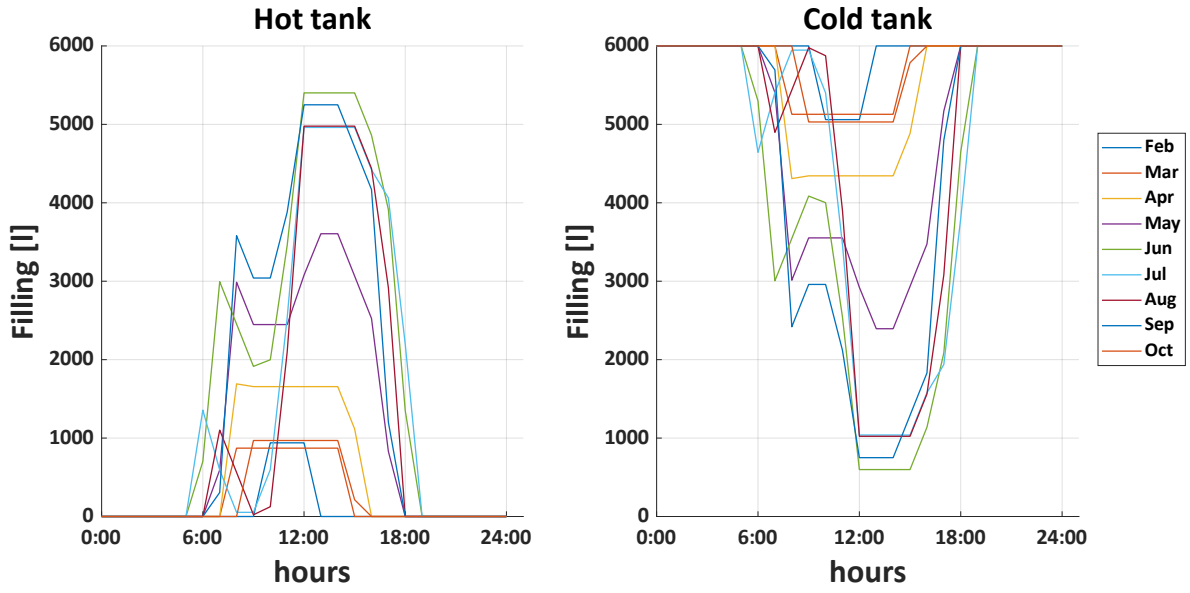

Figure 11. Daily profile of the storage tanks state of charge

3. Results and Discussion

In this section, first, the performance indexes used to show and discuss the results of the analysis are introduced. Then, a parametric analysis follows, to assess the optimal size of the solar collector capturing surface, and to observe the influence of the storage tanks' size on the performance. Eventually, the results of the simulated operation with the different working fluids are shown and discussed, using the performance indexes previously mentioned.

3.1. Performance indexes

Performance indexes, used to compare the different analysed configurations, are listed in Table 8; in particular the expander electric output power ($\dot{W}_{exp}$), the pump electric consumption ($\dot{W}_{pp}$), the net output power ($\dot{W}_{net}$), the back work ratio (BWR), the ORC efficiency (η_{tot}) are considered. Eventually,

the electricity production (E_{el}) is calculated as the hourly net output power ($\dot{W}_{net}$) multiplied by the ORC operation hours (t_{on}): both monthly and yearly values of the electricity production have been calculated.

Table 8. Performance indexes

Expander Output Power	$\dot{W}_{exp}$
ORC Pump Consumption	$\dot{W}_{pp}$
Net Output Power	$\dot{W}_{net} = \dot{W}_{exp} - \dot{W}_{pp}$
Back Work Ratio	$BWR = \frac{\dot{W}_{pp}}{\dot{W}_{exp}}$
ORC Efficiency	$\eta_{tot} = \frac{\dot{W}_{exp} - \dot{W}_{pp}}{\dot{Q}_{ev}}$
Electricity Production	$E_{el} = \sum \dot{W}_{net} \cdot t_{on}$

3.2. Parametric analysis: storage tanks and solar collector sizes

A parametric analysis has been carried out to assess the optimal size of the solar collector capturing surface, and to investigate the change in the performance when varying the size of the hot storage tanks, for a given micro-ORC system size.

In the first instance, a reference solar collector area of 32.25 m² (corresponding to 15 panels of the adopted model) was selected. To verify that both smaller and larger capturing surfaces would decrease the electricity production of the system, simulations were performed also for the solar collector area equal to 21.5 m² (10 panels) and 64.5 m² (30 panels). Furthermore, the storage tanks volume was varied from 0 to 12000 l with a step of 3000 l to investigate the influence of the tanks size on the performance.

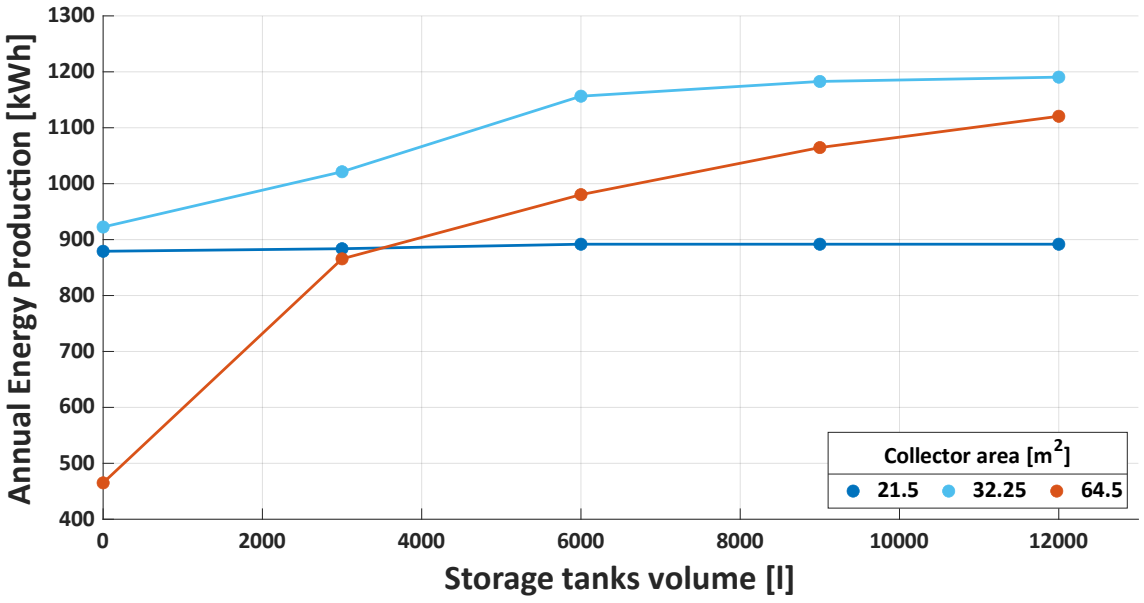

Figure 12. Yearly electricity production when varying the storage tank volume and the collector capturing surface

Figure 12 shows the simulated yearly electric energy produced by the system under the same boundary conditions (Table 7) and with the reference working fluid (R134a), with the different considered storage tanks volume and collector capturing surface values.

The increase of the hot storage tanks volume allows to progressively decouple the ORC loop operation from the hot circuit conditions: as a consequence, it results in a beneficial effect on the ORC performance and the electricity production. Indeed, when the irradiance is higher than the design value (i.e., 800 W/m^2 for the reference case), the buffer receives the thermal power surplus, which is released when the irradiation is lower. In this way, the optimal ORC boundary conditions, in terms of evaporator water inlet temperature, are provided for as long as possible.

Moreover, Figure 12 highlights that the annual electricity production is almost independent of the storage tanks volume when the collector area is small (21.5 m²). In this case, generally, the thermal power input does not reach the reference value of 16 kW, so the available heat from the collector is directly sent to the evaporator, and the storage thermal inertia is scarcely exploited (except when the irradiance is very low). Among the simulated size values of the solar collector, a capturing surface of 32.25 m² is proved to be the solution which grants the highest production. Nevertheless, also in this case, the electricity production approaches an asymptotic value because the storage capacity becomes too large to be completely exploited. A storage volume of about 6000 l thus proved to be a good compromise between dimensions and performance.

Further enlarging the solar collector surface (64.5 m²), under the assumption of keeping constant the water temperature glide, the water flow rate increases to accommodate the available thermal power input increase. However, due to the limited storage size, it becomes impossible to completely decouple the hot circuit and the ORC operation: as a consequence, the organic fluid mass flow rate must also be increased to face the thermal power input increase. Under these boundary conditions, the ORC is forced to work in off-design conditions, with a derating of the system performance (mainly due to the increase of the expander under-expansion losses and the pump consumption increase at the same time). In the view of the above, the penalization of the electric energy production is more significant with a smaller storage volume, due to the reduction in the storage thermal inertia.

It must be highlighted that the results of the collector size parametric analysis are specific for the case study of a kW-size ORC; coupling a larger collector surface with a larger ORC would lead instead to an increment in the electricity production. However, in this case, the dimensions would be no more compatible with the residential application.

3.3. Working fluids performance comparison

Results of the fluid assessment show that the expander electric power output is greater when using R134a as working fluid (Figure 13), since this fluid exhibits the highest isentropic enthalpy drop available to the expansion process. Indeed, R134a has a higher liquid density and viscosity than those presented by the other five fluids (Table 6), therefore it undergoes a lower pressure drop through the expander inlet valve. By using R134a, it is possible to obtain an average expander power output higher than 1000 W during the months between April and October, while with the low-GWP fluids it is not higher than about 600 W.

During the winter months (November, December and January), solar radiation never reaches a sufficient intensity to be exploited to produce electric energy.

Concerning the pump performance, R134a is the fluid with the maximum liquid viscosity (2.06 x10^{-4} Pa·s) and thus the minimum leakage losses at the pump meatus affecting volumetric flow. In addition, pump consumption is inversely proportional to the fluid density (Eq. (19)) (higher for R134a):

$$\dot{W}_{pp} = \frac{\dot{m}_{ORC} \cdot \Delta p}{\rho \cdot \eta} \tag{19}$$

However, pump consumption is higher in the case of the use of R134a (Figure 14), because a higher working fluid mass flow rate (Figure 15) is required since the imposed superheating degree is lower.

As a result, the system net power output is significantly higher when the plant behaviour is operated with R134a (Figure 16): values up to 500 W are reached, while with the low-GWP fluids values lower than 300 W occur all the year.

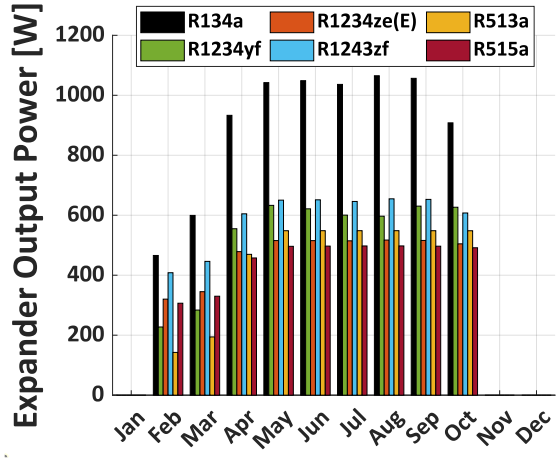

Figure 13. Monthly average expander output power

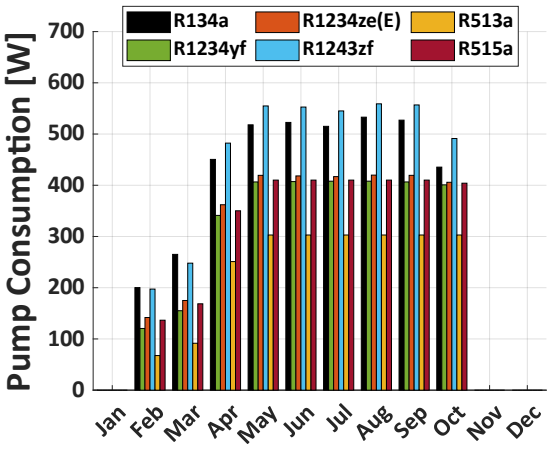

Figure 14. Monthly average pump consumption

Regarding the BWR (Figure 17), it reaches quite high values (always higher than 40%) with all the analyzed fluids due to the significant pump consumption, in line with typical values for ORC systems.

The highest efficiency (Figure 18) is reached with R134a (more than 2%). It must be highlighted that the analyzed system was properly designed to work with R134a and probably, redesigning the system for a new fluid would partially improve the overall performance when the new fluid is used. Nevertheless, it should be noticed that, considering the operating temperature levels of the sources of this application, the corresponding theoretical Carnot efficiency of the ORC system is lower than 14%.

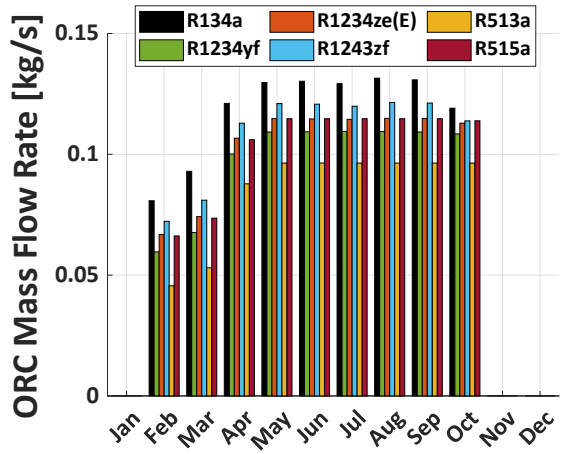

Figure 15. Monthly average ORC mass flow rate

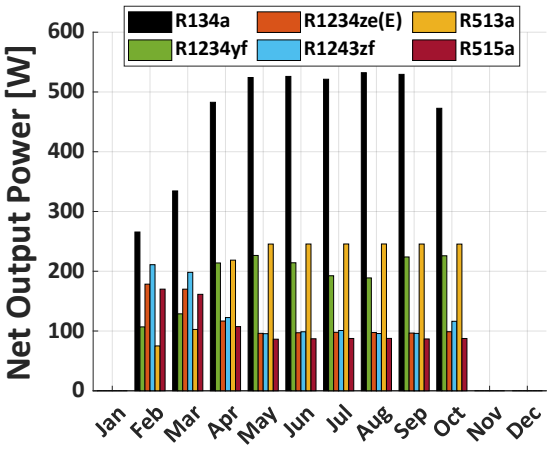

Figure 16. Monthly average net output power

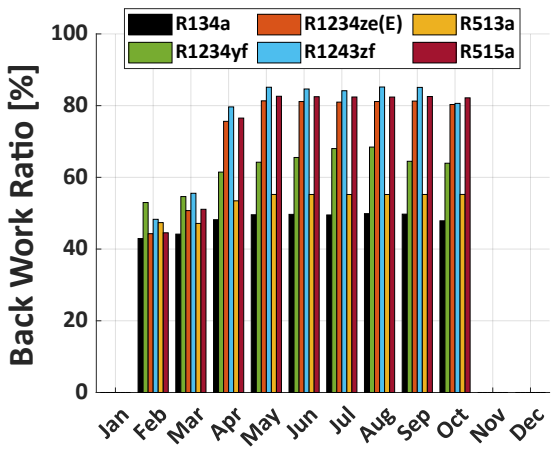

Figure 17. Monthly average back work ratio

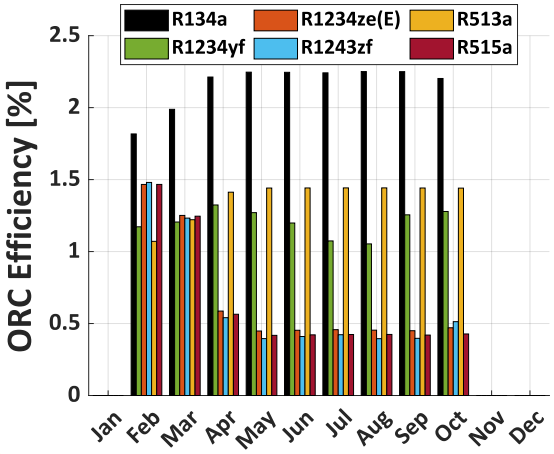

Figure 18. Monthly average ORC efficiency

Figure 19 shows the estimated monthly energy produced by the system. Annual electricity production of 1156.44 kWh is calculated, using R134a as working fluid; this energy production is about 30% more than the value estimated in the same solar radiation and ambient temperature conditions, and with the same micro-ORC power plant, but without including the hot water storage tanks (equal to 878.64 kWh per year, see Figure 12).

Considering a single-family user consumption value equal to 2996 kWh per year [47], the system would guarantee about 39% of the user demand (reduced to 29% in the case without thermal storage). According to the average price of electricity that occurred in Italy in 2019 (24.21 c€/kWh [48]), there would be an annual saving of € 280.

The reference micro-ORC test bench considered in this study is still a prototype not significant for the investment cost estimation. In order to estimate an approximate price of the whole simulated system (comprising the micro-ORC generator, the solar collector and the storage tanks), a market survey on similar systems has been carried out using web information and commercial components costs. In particular, regarding the ORC technology in the kW-size range, large uncertainties in cost estimation occur, because this is not very established on the market. According to the commercial information available from Air Square [49], the cost of micro-ORC systems can be estimated at approximately $ 10,000 per installed kW. Considering an average conversion efficiency from euro to dollar [50], and estimating the storage tanks and the solar collector cost respectively 6,000 € and 4,000 € [51], the complete simulated system would cost about17,000-19,000 €.

Thus the simulated system is still not competitive on the market, because it would have a pay-back period of more than 60 years, which is above the typically assumed system lifespan [52]. However, if it were possible to improve the efficiency of the system and increase the output power, it would be possible to save enough to allow a return on the initial investment in a few years.

An alternative solution consists in modifying the hot water circuit and increasing the solar radiation capturing surface to integrate the electric power with a thermal power production: an interesting layout, which could be investigated, would include the possibility of tapping hot water for a thermal user from the storage tanks. The hot circuit would be reintegrated upstream of the thermal solar collector with cold water, and the flow rate through it would be regulated in such a way as to guarantee the desired temperature at the inlet of the evaporator. Furthermore, by also including thermal production, it would be possible to turn off the ORC sub-system at lower solar radiation (and conversion efficiencies), but to exploit the system to satisfy a thermal request.

By using low-GWP fluids, the yearly electric energy production and the savings are lower: results are summarized in Table 9.

The performance comparison carried out in the current analysis emphasizes that, although there is an environmental benefit in terms of GWP, there is a penalty in terms of energy production when

conventional HFCs are replaced with alternative fluids. In the light of these results, it is evident that the research for fluids with a low environmental impact, which, at the same time, can ensure acceptable performance, is still fully open. However, the deep awareness of the causes of the low performance, obtained with low environmental impact working fluids, encourages further investigations.

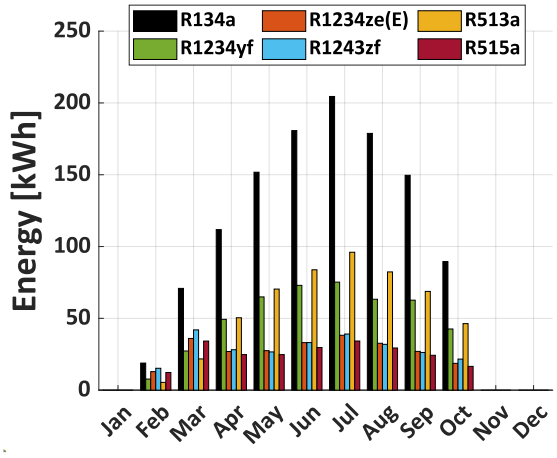

Figure 19. Output electric energy

Table 9. Estimated annual energy production

Working fluid	Electricity [kWh/year]	% of the satisfied requirement
R134a	1156.44	39.0%
R1234yf	466.01	16.0%
R1234ze(E)	252.92	8.0%
R1243zf	263.97	8.8%
R513A	525.21	17.5%
R515A	230.11	7.7%

4. Conclusions

A detailed semi-empirical steady-state simulation model of a kW-size micro-ORC prototypal system coupled with a commercial solar thermal collector is proposed. A performance comparative analysis on the estimated yearly electricity production for residential target with low-GWP working fluids to replace HFC-134a is provided.

The analysis was conducted on the reference small-scale test rig developed in the micro-generation laboratory of the University of Bologna (UNIBO-ORC test bench).

Semi-empirical models of all the main components, developed in the MATLAB environment, are detailed: the volumetric piston expander is simulated following a lumped parameters approach and validated for the reference reciprocating piston expander; the pump model provides the operating point of the machine by crossing the resistance curve of the circuit with the characteristic curve of the pump; the heat exchangers are modelled according to a lumped parameters moving boundary approach; the solar collector follows a 0-dimensional approach, which reproduces the energy balance between the incident solar radiation hitting the absorbing surface and the thermal power transferred to the hot water which supplies heat to the evaporator; a system of two storage tanks is included in the hot water circuit which feeds the evaporator.

Simulations were carried out considering a typical daily hourly profile of irradiation and ambient temperature (for the Italian town of Bologna) for each month: these profiles are obtained as monthly averages based on historical data. The system operation is evaluated at variable storage tanks size and solar collector area, identifying the couple of parameters that maximize the generated electric energy.

Then, the performances of the system are simulated by comparing its behaviour when the currently available working fluid, R134a, is replaced with five alternative low-GWP fluids: R1234yf, R1234ze(E), R1243zf and the blends R513A and R515A. Results highlight that the net power output produced with the low-GWP fluids is always lower than the one obtained with R134a (over 500 W) because of both a smaller isentropic enthalpy drop available in the expander and relatively higher pump consumption (due to the lower density of low-GWP fluids compared to R134a). Consequently, the BWR reaches higher values when the low-GWP fluids are used, while the highest global efficiency (more than 2%) is achieved with R134a.

It must be pointed out that an accurate micro-ORC system redesign and optimization would guarantee achieving higher components and overall performance with the alternative fluids analyzed. The yearly electricity production with R134a is estimated to be higher than 1150 kWh, fulfilling approximately 39% of the annual electric energy average single-family user requirement. Although the performed comparison might discourage the use of low-GWP fluids to replace HFC-134a, the urgency of the problems related to greenhouse gases emissions should push the research towards solutions which can increase the performance of both HFOs and blends, as they may effectively help to reduce the greenhouse gases impact.

Results could be extended including a deep and detailed economic analysis, providing a rigorous estimation of costs and return on the investment. Moreover, an optimization of the performance of the machines could be carried out, in order to include further results describing performance achievable based on state-of-art machines efficiencies.

Furthermore, the possibility to add thermal power production could be investigated too in the future. The analysis could be obtained by increasing the solar collector capturing surface and redesigning the system regulation strategy: in this way, it would be possible to satisfy a thermal demand, especially at lower solar radiation, when conversion efficiencies do not make the ORC convenient to use. Thus, the development of all the above-mentioned investigations represents a possible future extension of the current study.

CRediT roles

Maria Alessandra Ancona: supervision and investigation; Michele Bianchi: visualization and project administration; Lisa Branchini: conceptualization and formal analysis; Andrea De Pascale: funding acquisition, supervision and investigation, methodology, visualization; Francesco Melino: resources and conceptualization; Antonio Peretto: funding acquisition; Chiara Poletto: software, methodology, writing-original draft: Noemi Torricelli: data curation, methodology, writing-review and editing.

Acknowledgements

The Authors thank the 16th Conference on Sustainable Development of Energy Water and Environmental Systems - SDEWES, October 2021, Dubrovnik.

Funding sources

This research did not receive any specific grant from funding agencies in the public, commercial, or not-for-profit sectors.

References

[1] P.A. Østergaard, N. Duic, Y. Noorollahi, S. Kalogirou, Latest progress in Sustainable Development using renewable energy technology, Renew. Energy. 162 (2020) 1554–1562. https://doi.org/10.1016/J.RENENE.2020.09.124.

[2] B.S. Park, M. Usman, M. Imran, A. Pesyridis, Review of Organic Rankine Cycle experimental data trends, Energy Convers. Manag. 173 (2018) 679–691. https://doi.org/10.1016/j.enconman.2018.07.097.

[3] P.A. Østergaard, N. Duic, Y. Noorollahi, S.A. Kalogirou, Recent advances in renewable energy technology for the energy transition, Renew. Energy. 179 (2021) 877–884. https://doi.org/10.1016/J.RENENE.2021.07.111.

[4] J.S. Pereira, J.B. Ribeiro, R. Mendes, G.C. Vaz, J.C. André, ORC based micro-cogeneration systems for residential application - A state of the art review and current challenges, Renew. Sustain. Energy Rev. 92 (2018) 728–743. https://doi.org/10.1016/j.rser.2018.04.039.

[5] S. Quoilin, M. Van Den Broek, S. Declaye, P. Dewallef, V. Lemort, Techno-economic survey of Organic Rankine Cycle (ORC) systems, Renew. Sustain. Energy Rev. 22 (2013) 168–186. https://doi.org/10.1016/j.rser.2013.01.028.

[6] Rémi Dickes, A. Desideri, E. Casati, S. Quoilin, From 1885 to nowadays : a (short) techno-historical review of Solar Organic Rankine Cycle system, (2021) 1–8.

[7] P.A. Østergaard, N. Duic, Y. Noorollahi, H. Mikulcic, S. Kalogirou, Sustainable development using renewable energy technology, Renew. Energy. 146 (2020) 2430–2437. https://doi.org/10.1016/J.RENENE.2019.08.094.

[8] K. Soulis, D. Manolakos, E. Ntavou, G. Kosmadakis, R. Ike, T.P. Lefkippos, Preliminary operation assessment of a two-stage ORC engine combined with evacuated tube solar collectors throughout Greece, (2021) 1–9.

[9] Lorenzo Tocci, Tamas Pal, Ioannis Pesmazoglou, Benjamin Franchetti, Small Scale Organic Rankine Cycle (ORC): A Techno-Economic Review, Energies. (2017).

[10] S. Quoilin, M. Orosz, H. Hemond, V. Lemort, Performance and design optimization of a low-cost solar organic Rankine cycle for remote power generation, Sol. Energy. 85 (2011) 955–966. https://doi.org/10.1016/j.solener.2011.02.010.

[11] W. Lombardo, S. Ottaviano, L. Branchini, S. Vasta, A. De Pascale, A. Sapienza, A dynamic model of a solar driven trigeneration system based on micro-ORC and adsorption chiller prototypes, in: AIP Conf. Proc., American Institute of Physics Inc., 2019: p. 020098. https://doi.org/10.1063/1.5138831.

[12] F. Calise, M.D. D'Accadia, M. Vicidomini, M. Scarpellino, Design and simulation of a prototype of a small-scale solar CHP system based on evacuated flat-plate solar collectors and Organic Rankine Cycle, Energy Convers. Manag. 90 (2015) 347–363. https://doi.org/10.1016/j.enconman.2014.11.014.

[13] T.C. Roumpedakis, G. Loumpardis, E. Monokrousou, K. Braimakis, A. Charalampidis, S. Karellas, Exergetic and economic analysis of a solar driven small scale ORC, Renew. Energy. 157 (2020) 1008–1024. https://doi.org/10.1016/j.renene.2020.05.016.

[14] C. Kutlu, M.T. Erdinc, J. Li, Y. Wang, Y. Su, A study on heat storage sizing and flow control for a domestic scale solar-powered organic Rankine cycle-vapour compression refrigeration system, Renew. Energy. 143 (2019) 301–312. https://doi.org/10.1016/j.renene.2019.05.017.

[15] S. Quoilin, O. Dumont, K.H. Hansen, V. Lemort, Design, Modeling, and Performance Optimization of a Reversible Heat Pump/Organic Rankine Cycle System for Domestic Application, J. Eng. Gas Turbines Power. 138 (2016). https://doi.org/10.1115/1.4031004.

[16] Z. Liu, A. Romagnoli, P. Sapin, C. Markides, M. Mersch, Dynamic control strategies for a solar-ORC system using first-law dynamic and data-driven machine learning models, (2021) 1–14.

[17] M. Ciani Bassetti, D. Consoli, G. Manente, A. Lazzaretto, Design and off-design models of a hybrid geothermal-solar power plant enhanced by a thermal storage, Renew. Energy. 128 (2018) 460–472. https://doi.org/10.1016/j.renene.2017.05.078.

[18] J.L. Wang, L. Zhao, X.D. Wang, A comparative study of pure and zeotropic mixtures in low-temperature solar Rankine cycle, Appl. Energy. 87 (2010) 3366–3373. https://doi.org/10.1016/j.apenergy.2010.05.016.

[19] G. Qiu, Selection of working fluids for micro-CHP systems with ORC, Renew. Energy. 48 (2012) 565–570. https://doi.org/10.1016/j.renene.2012.06.006.
[20] R. Rayegan, Y.X. Tao, A procedure to select working fluids for Solar Organic Rankine Cycles (ORCs), Renew. Energy. 36 (2011) 659–670. https://doi.org/10.1016/j.renene.2010.07.010.
[21] B.F. Tchanche, G. Papadakis, G. Lambrinos, A. Frangoudakis, Fluid selection for a low-temperature solar organic Rankine cycle, Appl. Therm. Eng. 29 (2009) 2468–2476. https://doi.org/10.1016/j.applthermaleng.2008.12.025.
[22] M. Bianchi, L. Branchini, A. De Pascale, F. Melino, S. Ottaviano, A. Peretto, N. Torricelli, Performance modelling and greenhouse impact assessment of a micro-ORC energy system working with HFCs, low GWP fluids and mixtures, in: 100RES 2020 – Appl. Energy Symp., 2020.
[23] K. Yadav, A. Sircar, Selection of working fluid for low enthalpy heat source Organic Rankine Cycle in Dholera, Gujarat, India, Case Stud. Therm. Eng. 16 (2019) 100553. https://doi.org/10.1016/j.csite.2019.100553.
[24] J. Bao, L. Zhao, A review of working fluid and expander selections for organic Rankine cycle, Renew. Sustain. Energy Rev. 24 (2013) 325–342. https://doi.org/10.1016/j.rser.2013.03.040.
[25] I.H. Bell, P.A. Domanski, M.O. McLinden, G.T. Linteris, The hunt for nonflammable refrigerant blends to replace R-134a, Int. J. Refrig. 104 (2019) 484–495. https://doi.org/10.1016/J.IJREFRIG.2019.05.035.
[26] Y. Heredia-Aricapa, J.M. Belman-Flores, A. Mota-Babiloni, J. Serrano-Arellano, J.J. García-Pabón, Overview of low GWP mixtures for the replacement of HFC refrigerants: R134a, R404A and R410A, Int. J. Refrig. 111 (2020) 113–123. https://doi.org/10.1016/J.IJREFRIG.2019.11.012.
[27] F. Molés, J. Navarro-Esbrí, B. Peris, A. Mota-Babiloni, C. Mateu-Royo, R1234yf and R1234ze as alternatives to R134a in Organic Rankine Cycles for low temperature heat sources, in: Energy Procedia, Elsevier Ltd, 2017: pp. 1192–1198. https://doi.org/10.1016/j.egypro.2017.12.380.
[28] M. A. Ancona, M. Bianchi, L. Branchini, A. De Pascale, F. Melino, S. Ottaviano, A. Peretto, N. Torricelli, Performance prediction and design optimization of a kW-size reciprocating piston expander working with low-GWP fluids, (2019).
[29] X.D. Wang, L. Zhao, Analysis of zeotropic mixtures used in low-temperature solar Rankine cycles for power generation, Sol. Energy. 83 (2009) 605–613. https://doi.org/10.1016/j.solener.2008.10.006.
[30] G. Bamorovat Abadi, E. Yun, K.C. Kim, Experimental study of a 1 kw organic Rankine cycle with a zeotropic mixture of R245fa/R134a, Energy. 93 (2015) 2363–2373. https://doi.org/10.1016/j.energy.2015.10.092.
[31] M. Bianchi, L. Branchini, A. De Pascale, F. Melino, S. Ottaviano, A. Peretto, N. Torricelli, Replacement of R134a with low-GWP fluids in a kW-size reciprocating piston expander: Performance prediction and design optimization, Energy. 206 (2020) 118174. https://doi.org/10.1016/j.energy.2020.118174.
[32] M. Bianchi, L. Branchini, N. Casari, A. De Pascale, F. Melino, S. Ottaviano, M. Pinelli, P.R. Spina, A. Suman, Experimental analysis of a micro-ORC driven by piston expander for low-grade heat recovery, Appl. Therm. Eng. 148 (2019) 1278–1291. https://doi.org/10.1016/j.applthermaleng.2018.12.019.
[33] R. Dickes, O. Dumont, R. Daccord, S. Quoilin, V. Lemort, Modelling of organic Rankine cycle power systems in off-design conditions: An experimentally-validated comparative study, Energy. 123 (2017) 710–727. https://doi.org/10.1016/j.energy.2017.01.130.
[34] PDR: NIST Reference Fluid Thermodynamic and Transport Properties Database (REFPROP) Version 9 - SRD 23, (n.d.). https://data.nist.gov/od/id/ECBCC1C130222ED9E04306570681B10740 (accessed December 2, 2021).
[35] I. Garcia-Saez, J. Méndez, C. Ortiz, D. Loncar, J.A. Becerra, R. Chacartegui, Energy and economic assessment of solar Organic Rankine Cycle for combined heat and power generation in residential applications, Renew. Energy. 140 (2019) 461–476. https://doi.org/10.1016/j.renene.2019.03.033.
[36] Residential Heating Residential Cooling Heat Pumps Solar Thermal and Cylinders Commercial

Heating Commercial Cooling System Complementary Items PRODUCT CATALOGUE 2015 INTERNATIONAL MARKETS, (2015). www.riello.com (accessed December 2, 2021).
[37] M. Bianchi, L. Branchini, A. De Pascale, F. Melino, S. Ottaviano, A. Peretto, N. Torricelli, Application and comparison of semi-empirical models for performance prediction of a kW-size reciprocating piston expander, Appl. Energy. 249 (2019) 143–156. https://doi.org/10.1016/j.apenergy.2019.04.070.
[38] D. Ziviani, B.J. Woodland, E. Georges, E.A. Groll, J.E. Braun, W. Travis Horton, M. Van Den Broek, M. De Paepe, Development and a Validation of a Charge Sensitive Organic Rankine Cycle (ORC) Simulation Tool, (2015) 30. https://doi.org/10.3390/en9060389.
[39] R. Dickes, O. Dumont, L. Guillaume, S. Quoilin, V. Lemort, Charge-sensitive modelling of organic Rankine cycle power systems for off-design performance simulation, Appl. Energy. 212 (2018) 1262–1281. https://doi.org/10.1016/j.apenergy.2018.01.004.
[40] D. Ziviani, R. Dickes, V. Lemort, J.E. Braun, E.A. Groll, Effects of the Working Fluid Charge in Organic Rankine Cycle Power Systems: Numerical and Experimental Analyses, in: Org. Rank. Cycle Technol. Heat Recover., InTech, 2018. https://doi.org/10.5772/intechopen.78026.
[41] A. Giuffrida, Modelling the performance of a scroll expander for small organic Rankine cycles when changing the working fluid, Appl. Therm. Eng. 70 (2014) 1040–1049. https://doi.org/10.1016/j.applthermaleng.2014.06.004.
[42] Global Warming Potential Values, (2021). www.ipcc.ch (accessed November 23, 2021).
[43] Y. Khan, R.S. Mishra, Performance analysis of solar driven combined recompression main compressor intercooling supercritical CO2 cycle and organic Rankine cycle using low GWP fluids, Energy Built Environ. (2021) e00118. https://doi.org/10.1016/J.ENBENV.2021.05.004.
[44] UNI 10349 standards, (2016). http://store.uni.com/catalogo/index.php/uni-10349-1-2016.
[45] Panels inclination, (2010). https://www.aggiustatutto.it/varie/nozioni-varie/353-inclinazione-pannelli-fotovoltaici-solari-termici.html.
[46] Average daily monthly global solar radiation, on a horizontal surface, (2020). http://www.solaritaly.enea.it/CalcRggmmOrizz/Calcola.php.
[47] P.S. Ennio Macchi, Stefano Campanari, La climatizzazione a gas e ad azionamento termico, n.d.
[48] Electricity prices in Italy, (2020). https://www.qualenergia.it/articoli/come-vanno-i-prezzi-dellenergia-elettrica-in-italia-i-dati-dellautorita/.
[49] Micro-ORC price, (2018). https://airsquared.com/news/introducing-plug-play-micro-orc/.
[50] Cambio Euro Dollaro 2021 Storico - cambioeuro, (n.d.). https://www.cambioeuro.it/cambio-storico-dollaro-2021/.
[51] S.A. Kalogirou, R. Agathokleous, G. Barone, A. Buonomano, C. Forzano, A. Palombo, Development and validation of a new TRNSYS Type for thermosiphon flat-plate solar thermal collectors: energy and economic optimization for hot water production in different climates, Renew. Energy. 136 (2019) 632–644. https://doi.org/10.1016/J.RENENE.2018.12.086.
[52] M. Bianchi, L. Branchini, A. De Pascale, F. Melino, A. Peretto, D. Archetti, F. Campana, T. Ferrari, N. Rossetti, Feasibility of ORC application in natural gas compressor stations, Energy. 173 (2019) 1–15. https://doi.org/10.1016/J.ENERGY.2019.01.127.